



# **Geophysical Research Letters**

## RESEARCH LETTER

10.1002/2016GL072453

#### **Key Points:**

- Primary productivity increasing in the Pacific sector and decreasing in the Atlantic sector of the Southern Ocean
- Annual cycle in reflectance anomaly is in phase with chlorophyll concentration in the Atlantic Ocean and out of phase in the Pacific Ocean
- Monthly time series of primary production can be statistically predicted using partial least squares regression of the reflectance anomalies

#### **Supporting Information:**

• Supporting Information S1

#### Correspondence to:

M. Kahru, mkahru@ucsd.edu

#### Citation:

Kahru, M., Z. Lee, and B. G. Mitchell (2017), Contemporaneous disequilibrium of bio-optical properties in the Southern Ocean, *Geophys. Res. Lett.*, *44*, doi:10.1002/2016GL072453.

Received 27 DEC 2016 Accepted 13 MAR 2017 Accepted article online 15 MAR 2017

# Contemporaneous disequilibrium of bio-optical properties in the Southern Ocean

Mati Kahru<sup>1</sup>, Zhongping Lee<sup>2</sup>, and B. Greg Mitchell<sup>1</sup>

<sup>1</sup>Scripps Institution of Oceanography, University of California, San Diego, La Jolla, California, USA, <sup>2</sup>School for the Environment, University of Massachusetts Boston, Boston, Massachusetts, USA

**Abstract** Significant changes in satellite-detected net primary production (NPP,  $mgCm^{-2}d^{-1}$ ) were observed in the Southern Ocean during 2011–2016: an increase in the Pacific sector and a decrease in the Atlantic sector. While no clear physical forcing was identified, we hypothesize that the changes in NPP were associated with changes in the phytoplankton community and reflected in the concomitant bio-optical properties. Satellite algorithms for chlorophyll a concentration (Chl a,  $mgm^{-3}$ ) use a combination of estimates of the remote sensing reflectance  $Rrs(\lambda)$  that are statistically fitted to a global reference data set. In any particular region or point in space/time the estimate produced by the global "mean" algorithm can deviate from the true value. Reflectance anomaly (RA) is supposed to remove the first-order variability in  $Rrs(\lambda)$  associated with Chl a and reveal bio-optical properties that are due to the composition of phytoplankton and associated materials. Time series of RA showed variability at multiple scales, including the life span of the sensor, multiyear and annual. Models of plankton functional types using estimated Chl a as input cannot be expected to correctly resolve regional and seasonal anomalies due to biases in the Chl a estimate that they are based on. While a statistical model using  $RA(\lambda)$  time series can predict the times series of NPP with high accuracy ( $R^2 = 0.82$ ) in both Pacific and Atlantic regions, the underlying mechanisms in terms of phytoplankton groups and the associated materials remain elusive.

# 1. Introduction

The Southern Ocean (SO) has a critical role in the global carbon balance, accounting for nearly half of the annual oceanic uptake of anthropogenic carbon dioxide [Gruber et al., 2009]. The net primary production (NPP,  $mg C m^{-2} d^{-1}$ ) in the SO is an important component of the global "biological pump" through which carbon dioxide assimilated in the surface layer is transported to the deep ocean. Empirical and semiempirical algorithms [O'Reilly et al., 1998; Maritorena et al., 2002; Dierssen, 2010; Hu et al., 2012] are being used to estimate properties like surface chlorophyll a concentration (Chl a, mg m<sup>-3</sup>) which is the primary input to many models of water column net primary production (NPP, mg C m<sup>-2</sup> d<sup>-1</sup>) [e.g., Behrenfeld and Falkowski, 1997]. Both Chl a and NPP are "bulk" properties in a sense that they are sums of variable contributions by many phytoplankton groups. Differentiation between the contributions of these phytoplankton groups or plankton functional types (PFTs) is a major research direction due to their different biogeochemical roles. PFTs can be separated in remote sensing data according to the optical imprint of variations in cell size [e.g., Kostadinov et al., 2009] or pigmentation [e.g., Alvain et al., 2005; Bracher et al., 2009]. While PFT algorithms seem to work at global scales, they are problematic at regional scales. Abundance-based PFT algorithms use the estimate of the total surface Chl a to partition Chl a or NPP into fractions due to different size classes or PFTs [e.g., Brewin et al., 2010; Uitz et al., 2010]. If the Chl a estimate is biased, so are the PFT estimates based on these algorithms.

This paper tries to explain the changes in NPP in two regions of the Southern Ocean from around 2011 to present (2016) in terms of their bio-optical properties. While we were unable to explain these changes by environmental forcing functions (analysis in the supporting information), we hypothesized that the changes in NPP were related to concomitant changes in bio-optical variables which relate to phytoplankton size and composition. Reflectance anomaly (RA) is defined as a ratio of satellite-derived remote sensing reflectance ( $Rrs(\lambda)$ ,  $sr^{-1}$ ) to a reference spectrum for the corresponding Chl a level [ $Alvain\ et\ al.$ , 2005, 2008] is expected to reveal second-order bio-optical variability after removing the first-order variability associated with Chl a. We evaluated time series in RA from Moderate Resolution Imaging Spectroradiometer (MODIS)-Aqua (MODISA) and Visible Infrared Imaging Radiometer Suite (VIIRS) data including bands from 410 nm to 671 nm and their relationships with Chl a and NPP.

©2017. American Geophysical Union. All Rights Reserved.



# 2. Methods

Primary productivity was estimated using a modified version of the vertically generalized productivity model (VGPM) [Behrenfeld and Falkowski, 1997] by using input from the quasi-analytical QAA semianalytic algorithm [Lee et al., 2002, 2005]. The depth of the euphotic zone was estimated using the coefficients of bulk absorption and backscattering [Lee et al., 2007]. Instead of Chl a used in the standard VGPM, we used the absorption coefficient of phytoplankton at 443 nm derived from QAA. The model is hence called VGPM-QAA [Kahru et al., 2016]. Daily estimates using VGPM-QAA were merged from multiple sensors in order to minimize gaps due to clouds and satellite orbits. Alternative estimates of the monthly primary productivity using MODISA were obtained from http://www.science.oregonstate.edu/ocean.productivity and included those derived by the standard VGPM and the carbon-based productivity model (CbPM) [Behrenfeld et al., 2005; Westberry et al., 2008].

Time series were created as mean values for the Pacific (37.25–45.5°S, 177.25–84°W) and Atlantic (40–53°S, 30°W–25°E) domains.

In order to characterize changes in the bio-optical properties we used reflectance anomalies (RA) proposed by Alvain and coauthors as input to the PHYSAT method of distinguishing PFTs [Alvain et al., 2005, 2008, 2012]. It is expected that by removing the first-order effects associated with Chl a from the normalized water leaving radiance  $(nLw(\lambda), mW \text{ cm}^{-2} \mu m^{-1} \text{ sr}^{-1})$  the remaining variations contain information on bio-optical properties due to varying contributions by different PFTs and the associated materials. We applied the same idea to remote sensing reflectance  $(Rrs(\lambda), sr^{-1})$  and used equally distributed bins of Chl a in log10 rather than in linear scale. RA( $\lambda$ ) of a pixel is therefore  $Rrs(\lambda)$  divided by a reference value,  $RrsRef(\lambda)$  that is the mean  $Rrs(\lambda)$ of all pixels with the same concentration of the standard Chl a estimate (chlor\_a). We calculated RA( $\lambda$ ) using daily level-3 data sets of  $Rrs(\lambda)$  at 9 km nominal resolution from MODISA (version 2014.0.1) and VIIRS (version 2014.01.2). Daily data sets of  $Rrs(\lambda)$  and Chl a ( $chlor_a$ , mg m<sup>-3</sup>) were obtained from the NASA Ocean Color Web (http://oceancolor.gsfc.nasa.gov). In step 1, reference spectra  $RrsRef(\lambda)$  were generated for 100 equally distributed bins of log10-transformed chlor\_a using daily data sets during the lifetime of a sensor (2002 to 2016 for MODISA and 2012 to 2016 for VIIRS) in the Southern Ocean between 40 and 60° S. Chl a bins were assumed to be in the interval from -3 to 2 in log10 units with a step of 0.05 (corresponding to a linear range from 0.001 to 100 mg m<sup>-3</sup>). In step 2, daily RA( $\lambda$ ) values were calculated by dividing the  $Rrs(\lambda)$  value in each pixel to the respective reference value corresponding to the estimated Chl a bin.

Partial least squares (PLS) regressions as implemented in the PLS1 routine of the *NMathStats* 4.2 numerical libraries (http://www.centerspace.net) were used to predict NPP from a set of RA bands.

## 3. Results

Time series of NPP derived with the merged, multisensor VGPM-QAA method [Kahru et al., 2016] showed a pattern of change during 2011–2016 in the Southern Ocean (Figure 1): an increase in the Pacific sector and a decrease in the Atlantic sector. The domains were chosen as coherent areas showing increase or decrease, respectively (Figure 1a). The increase in the annual maximum of the monthly average NPP from 2011 to 2016 was 35% in the Pacific domain (from 380 to 515 mg C m $^{-2}$  d $^{-1}$ ), and the corresponding decrease in the Atlantic domain was -23% (from 694 to 536 mg C m $^{-2}$  d $^{-1}$ ). When averaged over 2011–2013 and 2014–2016, respectively, the increase in the annual monthly maximum in the Pacific domain was 14% and the decrease in the Atlantic domain was -15%. Comparable values using alternative estimates from http://www.science.oregonstate.edu/ocean.productivity were 11% and -16% for VGPM and 5% and -20% using CbPM. The observed changes in surface Chl a were approximately similar to the changes in NPP (Figures 1d and 1e).

In spite of being normalized to the mean reflectance at the corresponding Chl *a* level, time series of RA show distinct variability at multiple scales, most notably at the annual scale. RA of the blue band, RA\_443, also shows a significant (*F* test at 95% level) long-term decreasing trend in the annual minima in the Pacific domain (Figure 2a) and in both the annual minima and the annual maxima in the Atlantic domain (Figure 2b). While the existence of such a long-term trend may be indicative of a calibration problem with the aging MODISA sensor, a similar decreasing trend is visible in the VIIRS data sets (Figures 2c and 2d) but the VIIRS data set is too short for the respective trend to be statistically significant. The annual cycles of

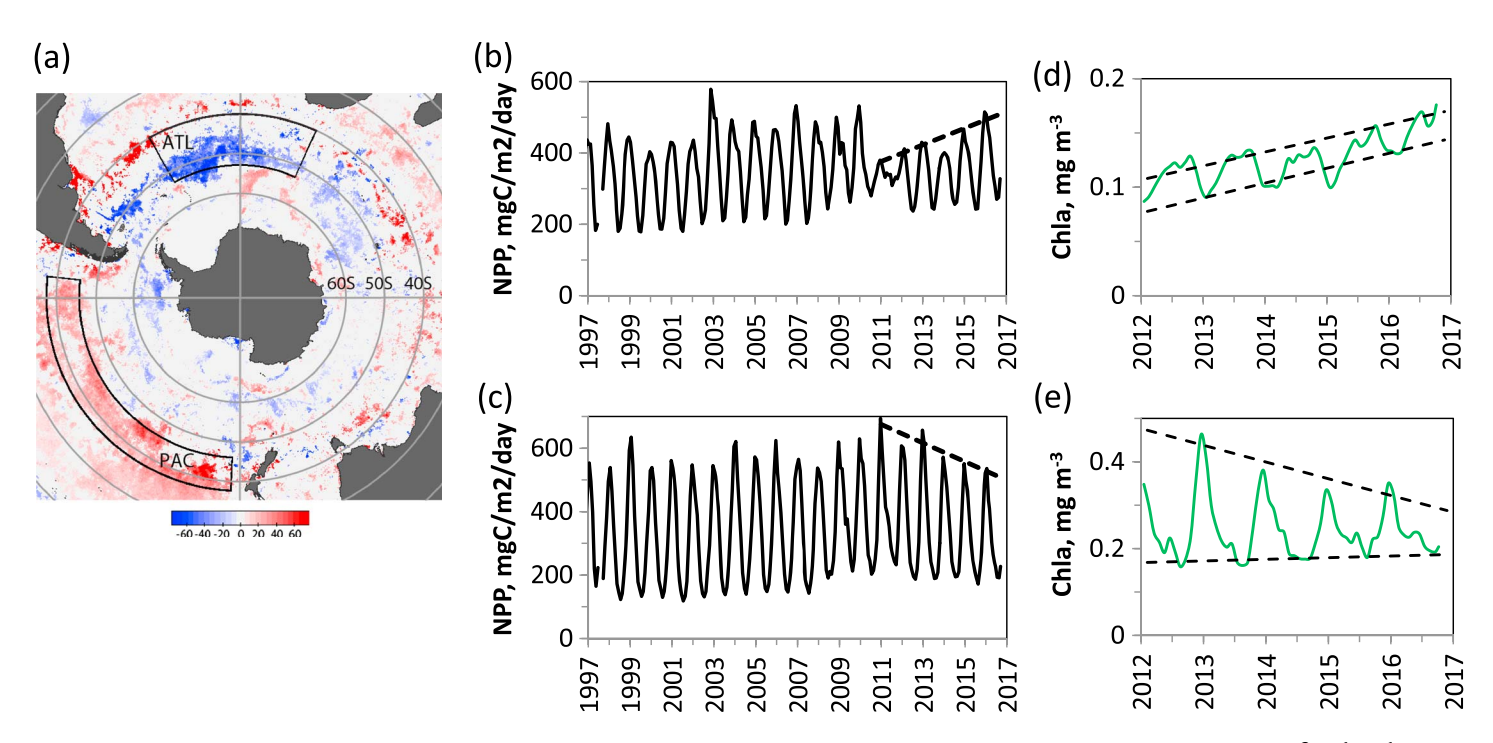


**Figure 1.** Time series of NPP merged from multiple sensors: (a) spatial distribution of the Sen slope for monthly values of NPP  $(mg C m^{-2} d^{-1} yr^{-1})$  during December-January-February in 2011–2016 and the Pacific (PAC) and Atlantic (ATL) domains. Slopes not significantly (p = 0.05) different from 0 are white. Monthly time series of NPP in the (b) Pacific and (c) Atlantic domains. Time series of the standard NASA surface Chl a (chlor\_a) derived with VIIRS in the (d) Pacific and (e) Atlantic domains. The dashed black lines are linear regressions through respective annual maxima (Figures 1b and 1c) or maxima and minima (Figures 1d and 1e).

RA\_443 are in the same phase with Chl *a* in the Atlantic but in the opposite phase in the Pacific (Figures 2c and 2d). The annual Chl *a* maximum occurs during the austral spring in the Pacific domain and during the austral summer in the Atlantic domain. The time series of RA\_443 did not show any peculiar changes that might be correlated with the changes in NPP during 2011–2016. However, temporal changes in RA of the approximately 490 nm band (RA\_488 of MODISA and RA\_486 of VIIRS, Figure 3) did show peculiar changes

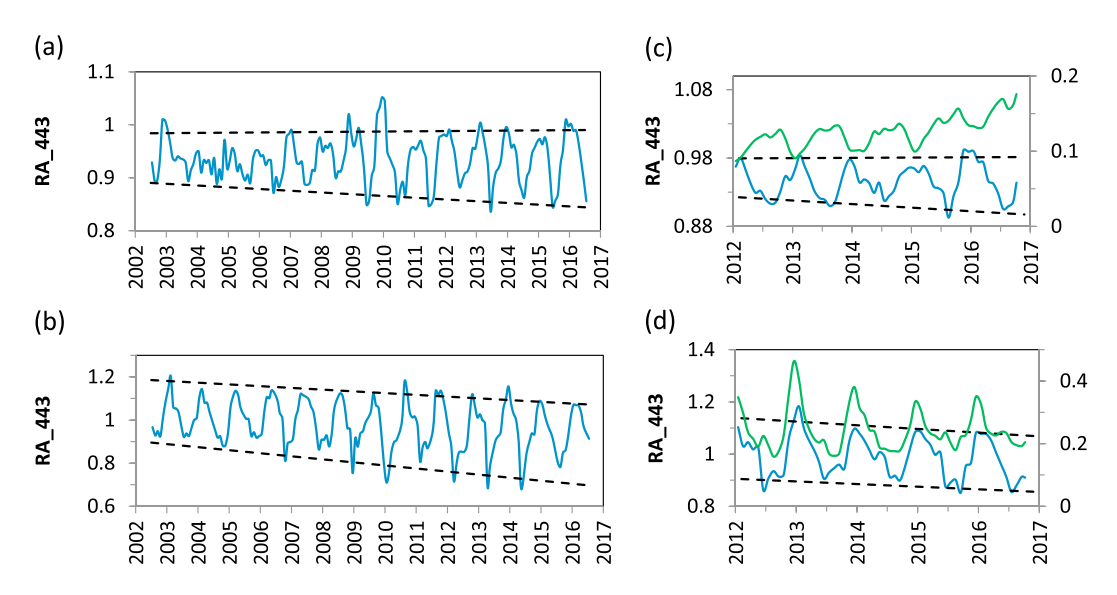


**Figure 2.** Time series of the monthly mean RA\_443 derived from (a, b) MODISA and (c, d) VIIRS in the Pacific (Figures 2a and 2c) and Atlantic (Figures 2b and 2d). For comparison, the respective monthly VIIRS ChI a time series are shown in green (mg m<sup>-3</sup>, right axis). Dashed black lines are linear regressions through the respective annual RA minima and maxima.

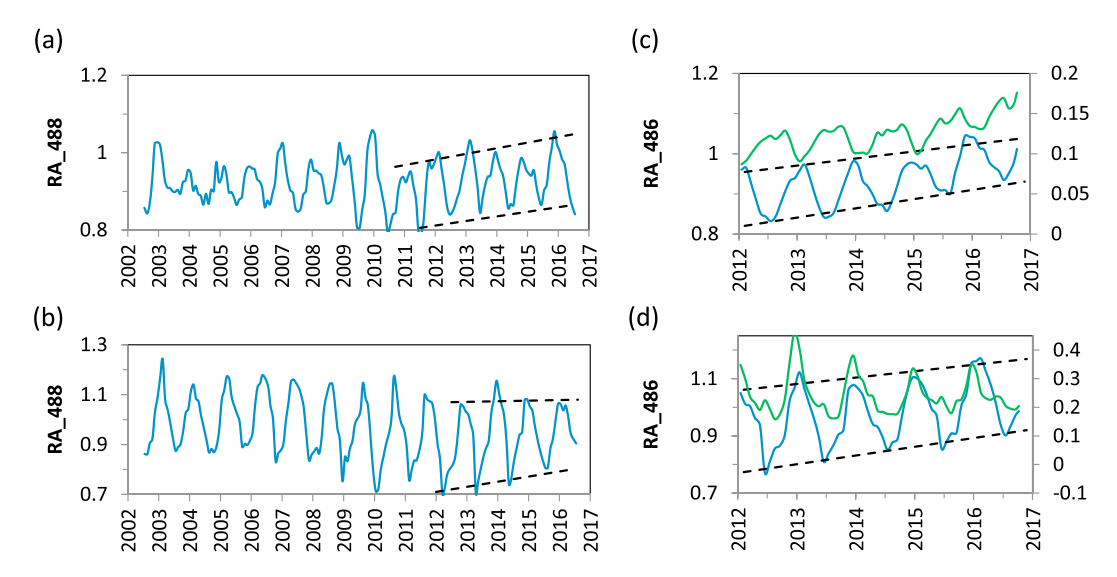


**Figure 3.** Time series of the monthly mean RA\_488 from (a, b) MODISA and RA\_486 from (c, d) VIIRS in the Pacific (Figures 3a and 3c) and Atlantic (Figures 3b and 3d). For comparison, the respective monthly VIIRS ChI *a* time series are shown in green (mg m<sup>-3</sup>, right axis). Dashed black lines are linear regressions through the respective annual RA minima and maxima.

in 2011–2016. In both domains the respective RA\_488 and RA\_486 values tended to increase in 2011–2016. In the Pacific domain the increase in RA\_488 and RA\_446 was similar to the increase in Chl *a* but seasonally out of phase (Figure 3c). In the Atlantic domain the trend of decreasing austral summer Chl *a* maxima in 2011–2016 was mirrored by the increasing winter RA\_488 and RA\_486 minima. The summer maximum in MODISA RA\_488 was flat (Figure 3b) during 2011–2016, but the VIIRS RA\_486 summer maxima showed an increase (Figure 3d) that was statistically not significant. As with RA\_443, the interannual changes in RA\_488 detected with MODISA were generally supported by the corresponding estimates from VIIRS. However, the time series of 2011–2016 were too short to prove statistical significance.

 $Rrs(\lambda)$  of the green band (Rrs(547) for MODISA and Rrs(551) for VIIRS) is used as the denominator in the empirical band ratio Chl a algorithms. During the 2011–2016 period RA of the green band showed trends that were similar but less expressed to those of RA\_486 and RA\_488, respectively. There was a slight increase in the Pacific domain but no significant change in the Atlantic domain. As with the other RA bands, the RA of the green band was in opposite phase with Chl a in the Pacific and in phase with Chl a in the Atlantic. Due to the low  $Rrs(\lambda)$  and higher relative errors, the annual cycle of RA of the green band was weaker and noisier, particularly in the Pacific domain.

The difference between the Pacific and the Atlantic domains is best illustrated by their opposite correlation of RA\_443 with Chl *a* (Figures 4a and 4b): negative in the Pacific and positive in the Atlantic. In spite of the opposite phase in the annual cycle between the RA bands and Chl *a* in the Pacific domain (Figures 2 and 3), a significant negative correlation was present only for the 443 nm band of RA (Figure 4c). For the other bands the negative correlation disappeared due to slight mismatches of the annual cycles. In contrast, in the Atlantic the significant positive correlation with Chl *a* due to the in-phase annual cycle was significant for all RA bands except for RA\_671 (Figure 4c). The correlations of the RA bands with NPP are more uniform: in both domains all RA bands except RA\_671 are positively correlated with NPP (Figure 4d).

While the correlations between the time series of individual bands of RA and NPP are lower in the Pacific than in the Atlantic domains, a combination of RA bands is a good predictor of NPP in both domains. The monthly time series of NPP (merged from MODISA and VIIRS) can be predicted using partial least squares regressions from the five VIIRS RA bands (410, 443, 486, 551, and 670 nm) with an  $R^2 = 0.82$  for both Pacific and Atlantic domains (Figure 5). The strongest contribution in the Pacific domain was from RA\_486 (followed by 443 and 410 nm) and from RA\_551 in the Atlantic domain (followed by 486 and 443 nm). RA\_670 had the least influence in both domains. Surprisingly, RA\_443 did not have the strongest influence in either of the domains.

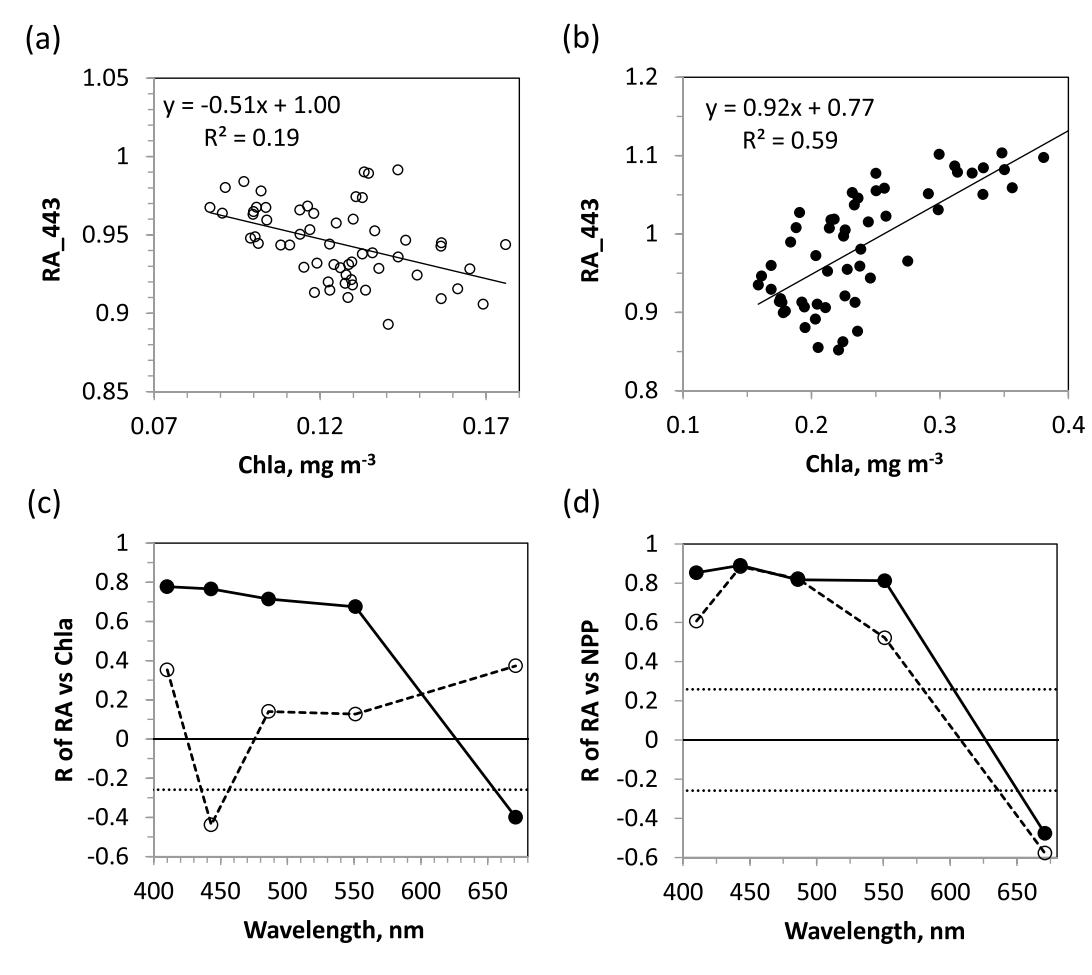


Figure 4. Scatterplots of the VIIRS monthly mean RA\_443 against Chl a in the (a) Pacific and (b) Atlantic domains. Wavelength dependence of the correlation coefficient (R) between monthly values of (c) RA( $\lambda$ ) and Chl a and (d) RA( $\lambda$ ) and NPP in the Pacific domain (open circles and dotted curve) and Atlantic domain (filled circles and solid line). Dotted lines show the 95% confidence lines of R = 0.

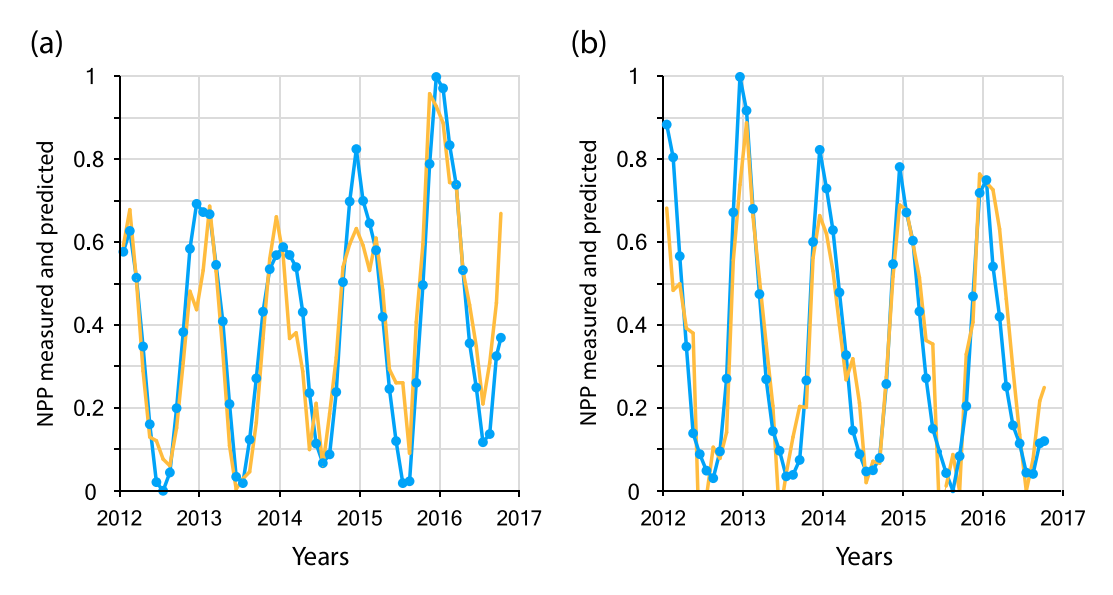


Figure 5. Partial least squares regressions predicting NPP merged from MODISA and VIIRS (blue line and dots) using VIIRS RA\_410, RA\_443, RA\_486, RA\_551, and RA\_671 with one factor (yellow line) with  $R^2 = 0.82$  for both the (a) Pacific and the (b) Atlantic domains. Both input and output variables were normalized to be between 0 and 1.



#### 4. Discussion

The time series of NPP created by the VGPM-QAA method was merged from multiple sensors (Ocean Color and Temperature Scanner, Sea-viewing Wide Field-of-view Sensor, Medium-Resolution Imaging Spectrometer, MODISA, and VIIRS). During the 2012–2016 period MODISA and VIIRS ocean color data were used in NPP calculations, while PAR was merged from MODISA, MODIS-Terra, and VIIRS. The potential explanation for the change in NPP due to a degradation of the radiometric calibration of the aging MODISA sensor cannot be ruled out but does not seem likely as the respective variables from VIIRS showed similar changes to those of MODISA. Pixel-to-pixel comparisons of the daily MODISA *Rrs* values with VIIRS (not shown) also showed reasonably good correspondence between MODISA and VIIRS.

By definition, the normalized water leaving radiance used in the calculation of  $Rrs(\lambda)$  is the radiance leaving the water surface if the Sun were at zenith, in absence of atmosphere, and when the Earth is at its mean distance from the Sun [Gordon and Wang, 1994]. Therefore, Rrs(\(\lambda\)) should be independent of the Sun and sensor geometry, and the annual  $Rrs(\lambda)$  cycle should only be a function of in-water properties like absorption and scattering. However, in practice, the normalization is convolved with atmospheric correction that has a seasonal component. In the calculation of RA we are additionally normalizing  $Rrs(\lambda)$  to its mean value at corresponding Chl a. Therefore, even if there is a significant annual cycle in Chl a, the annual cycle in RA should be small assuming that the in-water properties covary with Chl a. In reality, bands of RA have strong annual cycles that are comparable to the annual cycle of Chl a. Assuming that  $Rrs(\lambda)$  is fully normalized, this indicates that normalizing to the mean  $Rrs(\lambda)$  at estimated Chl a level has no effect on removing additional variance. It is likely that there is an annual cycle in the bias of the estimated Chl a and/or that the bio-optical properties have an annual cycle that is separate from the annual cycle in Chl a. It is not clear why the annual cycles in RA are in phase with Chl a in the Atlantic but in the opposite phase in the Pacific, but it may be related to the different ChI a levels. It is known that the annual and interannual changes in ChI a are more closely related to the particle backscattering spectral dependency (i.e., particle size) than to the magnitude of backscatter [Vantrepotte et al., 2011].

In our calculation of RA( $\lambda$ ),  $Rrs(\lambda)$  is normalized to the mean  $Rrs(\lambda)$  at the same Chl a level estimated by the sensor in the Southern Ocean between 40 and 60° S during the lifetime of the sensor. Due to regional differences in bio-optical characteristics of phytoplankton and the associated materials, the regional mean of RA( $\lambda$ ) can be consistently different from unity. For example, in our Pacific domain RA( $\lambda$ ) were predominantly below 1.0, while in the Atlantic domain RA( $\lambda$ ) values were distributed above and below 1.0 (Figure 4).

It is difficult to explain the long-term decreasing trend in RA\_443, particularly in its annual minima that was observed in both MODISA and VIIRS data. Also, there does not seem to be an obvious relationship between changes in RA\_443 and changes in NPP in 2011–2016. This seems to be counterintuitive as the estimation of NPP in the VGPM-QAA model is through the absorption coefficient of phytoplankton at 443 nm. In contrast, changes in RA\_488 (MODISA) and RA\_486 (VIIRS) do show peculiar features during the period of interest 2011–2016, e.g., an increase in the annual minima in both Pacific and Atlantic domains (Figures 3a and 3b) that seem to be related to the changes in NPP in 2011–2016. Also, in the partial least squares regression RA\_486 has the dominant influence on NPP in the Pacific and second most dominant influence in the Atlantic domain. The difference between the Pacific and the Atlantic in the strongest RA contribution in the PLS regression (RA\_486 versus RA\_551) and the consistently lower RA( $\lambda$ ) in the Pacific and higher RA( $\lambda$ ) in the Atlantic indicate that variations in the absorption dominate in the Pacific but variations in backscatter dominate in the Atlantic. This is indicative of a bigger role of coccolithophores in the Atlantic [e.g., *Balch et al.*, 2005].

When normalizing  $Rrs(\lambda)$  to its reference value at a specified Chl a level, we have assumed that the estimated Chl a represents a true value. However, the regional and seasonal bias in the estimate of Chl a can be twofold or more [e.g., Kahru and Mitchell, 2010]. Therefore, the bias in Chl a will be transferred to RA. If the bias has an annual cycle, then that may be one factor causing the annual cycle in RA. Evaluation of the relationships between RA( $\lambda$ ) and Chl a is complicated by the fact that the current standard Chl a algorithm ( $chlor_a$ ) is a blend: it uses a band ratio algorithm (OCx) at Chl  $a > 0.3 \, \mathrm{mg \, m^{-3}}$ , color index algorithm (ClA) below 0.175 mg m<sup>-3</sup>, and a linear blend of the two in between 0.175 and 0.3 mg m<sup>-3</sup> [Hu et al, 2012; Hu, personal communication, 2016]. Therefore, as Chl a values are predominantly below 0.2 mg m<sup>-3</sup> in the Pacific domain, the estimates are produced by the ClA. In the Atlantic domain the austral summer maxima are above



 $0.25 \,\mathrm{mg}\,\mathrm{m}^{-3}$  and are therefore mostly produced with the band ratio algorithm. As a consequence of the decreasing trend in RA\_443, particularly during the austral summer Chl a maximum, it is likely that the maximum band ratio algorithm is switching from using the Rrs(443)/Rrs(547) ratio to Rrs(488)/Rrs(547).

We hypothesize that the observed changes in RA( $\lambda$ ) and the associated changes in bulk properties (ChI a, NPP) are a reflection of the state of contemporaneous disequilibrium and reflect multiscale deviations from the statistically mean conditions that are assumed in the global empirical algorithms. A similar concept was proposed nearly five decades ago [*Richerson et al.*, 1970] to characterize the state of the phytoplankton community in a continuous state of change, balancing a diverse assemblage of species with different properties and physiological adaptations.

#### 5. Conclusions

A multiyear increase in NPP in the Pacific sector and a decrease in the Atlantic sector of the Southern Ocean during 2011–2016 period were observed based in satellite estimates and were hypothesized to be related to changes in phytoplankton composition. In spite of being normalized to the mean  $Rrs(\lambda)$  at the corresponding Chl a value, time series of RA( $\lambda$ ) exhibit strong annual cycles. In addition to the annual changes, time series of RA show significant variability at other scales. The long-term trend in RA\_443 observed over ~15 years is difficult to explain. RA( $\lambda$ ) values reflect changes in the phytoplankton community and nonliving substances in the water. As the multiscale variabilities observed in RA( $\lambda$ ) are difficult to explain, using RA( $\lambda$ ) as the input variable for detecting plankton functional types seems to be questionable at regional scales. While the monthly time series of NPP can be statistically predicted using partial least squares regression of RA( $\lambda$ ), the real mechanisms are unclear. The bio-optical properties of the ocean are highly variable at many spatial and temporal scales and can be conceptually described as a system in a contemporaneous disequilibrium. Current standard ocean color algorithms that are using statistical fits to global mean conditions are not capable of properly representing regional and/or seasonal anomalies.

#### Acknowledgments

We thank NASA Ocean Color Processing Group for satellite data (see section 2). Financial support was provided by NASA grants NNX14AL80G, NNX14AM15G, and NNX15AC98G.

## References

- Alvain, S., C. Moulin, Y. Dandonnea, and F. M. Breon (2005), Remote sensing of phytoplankton groups in case1 waters from global SeaWiFS imagery, *Deep Sea Res., Part I, 52*, 1989–2004, doi:10.1016/j.dsr.2005.06.015.
- Alvain, S., C. Moulin, Y. Dandonneau, and H. Loisel (2008), Seasonal distribution and succession of dominant phytoplankton groups in the global ocean: A satellite view. *Global Biogeochem. Cycles.* 22. GB3001, doi:10.1029/2007GB003154.
- Alvain, S., H. Loisel, and D. Dessailly (2012), Theoretical analysis of ocean color radiances anomalies and implications for phytoplankton groups detection in case1 waters, *Opt. Express*, 20, 1070–1083, doi:10.1364/OE.20.001070.
- Balch, W. M., H. R. Gordon, B. C. Bowler, D. T. Drapeau, and E. S. Booth (2005), Calcium carbonate measurements in the surface global ocean based on Moderate-Resolution Imaging Spectroradiometer data, *J. Geophys. Res., 110*, C07001, doi:10.1029/2004JC002560.
- Behrenfeld, M. J., and P. G. Falkowski (1997), Photosynthetic rates derived from satellite based chlorophyll concentration, *Limnol. Oceanogr.*, 42, 1–20.
- Behrenfeld, M. J., E. Boss, D. A. Siegel, and D. M. Shea (2005), Carbon-based ocean productivity and phytoplankton physiology from space, *Global Biogeochem. Cycles*, 19, GB1006, doi:10.1029/2004GB002299.
- Bracher, A., M. Vountas, T. Dinter, J. P. Burrows, R. Rottgers, and I. Peeken (2009), Quantitative observation of cyanobacteria and diatoms from space using PhytoDOAS on SCIAMACHY data, *Biogeosciences*, 6, 751–764.
- Brewin, R. J. W., S. Sathyendranath, T. Hirata, S. J. Lavender, R. Barciela, and N. Hardman-Mountford (2010), A three-component model of phytoplankton size class for the Atlantic Ocean, *Ecol. Model.*, 221, 1472–1483.
- Dierssen, H. M. (2010), Perspectives on empirical approaches for ocean color remote sensing of chlorophyll in a changing climate, *Proc. Natl. Acad. Sci. U.S.A.*, 107, 17,073–17,078, doi:10.1073/pnas.0913800107.
- Gordon, H. R., and M. Wang (1994), Retrieval of water-leaving radiance and aerosol optical thickness over the oceans with SeaWiFS: A preliminary algorithm, *Appl. Opt.*, *33*, 443–452.
- Gruber, N., et al. (2009), Oceanic sources, sinks, and transport of atmospheric CO2, *Global Biogeochem. Cycles*, 23, GB1005, doi:10.1029/
- Hu, C., Z. Lee, and B. Franz (2012), Chlorophyll a algorithms for oligotrophic oceans: A novel approach based on three-band reflectance difference, J. Geophys. Res., 117, C01011, doi:10.1029/2011JC007395.
- Kahru, M., and B. G. Mitchell (2010), Blending of ocean colour algorithms applied to the Southern Ocean, *Remote Sens. Lett.*, 1(2), 119–124, doi:10.1080/01431160903547940.
- Kahru, M., Z. Lee, B. G. Mitchell, and C. D. Nevison (2016), Effects of sea ice on satellite-detected primary production in the Arctic Ocean, *Biol. Lett.*, 12, 20160223, doi:10.1098/rsbl.2016.0223.
- Kostadinov, T. S., D. A. Siegel, and S. Maritorena (2009), Retrieval of the particle size distribution from satellite ocean color observations, J. Geophys. Res., 114, C09015, doi:10.1029/2009JC005303.
- Lee, Z. P., K. L. Carder, and R. A. Arnone (2002), Deriving inherent optical properties from water color: A multiband quasi-analytical algorithm for optically deep waters, *Appl. Opt.*, 41, 5755–5772.
- Lee, Z. P., M. Darecki, K. L. Carder, C. O. Davis, D. Stramski, and W. J. Rhea (2005), Diffuse attenuation coefficient of downwelling irradiance: An evaluation of remote sensing methods, *J. Geophys. Res.*, 110, C02017, doi:10.1029/2004JC002573.



# **Geophysical Research Letters**

- Lee, Z. P., A. Weidemann, J. Kindle, R. Arnone, K. L. Carder, and C. Davis (2007), Euphotic zone depth: Its derivation and implication to ocean-color remote sensing, *J. Geophys. Res.*, 112, C03009, doi:10.1029/02006JC003802.
- Maritorena, S., D. A. Siegel, and A. R. Peterson (2002), Optimization of a semianalytical ocean color model for global-scale applications, *Appl. Opt.*, *41*, 2705–2714, doi:10.1364/AO.41.002705.
- O'Reilly, J. E., S. Maritorena, B. G. Mitchell, D. A. Siegel, K. L. Carder, S. A. Garver, M. Kahru, and C. R. McClain (1998), Ocean color chlorophyll algorithms for SeaWiFS, J. Geophys. Res., 103, 24,937–24,953, doi:10.1029/98JC02160.
- Richerson, P., R. Armstrong, and C. R. Goldman (1970), Contemporaneous disequilibrium, a new hypothesis to explain the "paradox of plankton", *Proc. Natl. Acad. Sci. U.S.A.*, 67, 1710–1714.
- Uitz, J., H. Claustre, B. Gentili, and D. Stramski (2010), Phytoplankton class-specific primary production in the world's oceans: Seasonal and interannual variability from satellite observations, *Global Biogeochem. Cycles*, 24, GB3016, doi:10.1029/2009GB003680.
- Vantrepotte, V., H. Loisel, F. Mélin, D. Desailly, and L. Duforêt-Gaurier (2011), Global particulate matter pool temporal variability over the SeaWiFS period (1997–2007), Geophys. Res. Lett, 38, L02605, doi:10.1029/2010GL046167.
- Westberry, T., M. J. Behrenfeld, D. A. Siegel, and E. Boss (2008), Carbon-based primary productivity modeling with vertically resolved photoacclimation, *Global Biogeochem. Cycles*, 22, GB2024, doi:10.1029/2007GB003078.